Power Scaling in a Diode-End-Pumped Multisegmented Nd:YVO_4 Laser With Double-Pass Power Amplification

Yu-Jen Huang, Wei-Zhe Zhuang, Kuan-Wei Su, and Yung-Fu Chen

***Abstract*—We demonstrate a high-power master oscillator power amplifier with the double-pass configuration based on the specially designed multisegmented Nd:YVO_4 crystals. A powerful mathematical technique on the basis of the Fourier eigenfunction expansion method is developed for precisely calculating the temperature distribution inside the gain medium. A seed Nd:YVO_4 oscillator under dual-end pumping is subsequently constructed for efficiently emitting the output power of up to 50 W. Moreover, under a total incident pump power of 244 W at 808 nm, as high as 108 W of the output power at 1064 nm is further generated in our developed master oscillator power amplifier system. Theoretical and experimental results clearly reveal that the gain medium with multiple doping concentrations is practically valuable for constructing a high-power end-pumped laser without bringing in significantly thermal effects.**

***Index Terms*—Diode-pumped laser, high-power laser, master oscillator power amplifier, multisegmented laser crystal.**

I. Introduction

OVER the past few decades, high-power solid-state lasers were rapidly developed because they are useful for many scientific studies and industrial applications [1]–[3]. For the extension of the power scale-up in the end-pumped oscillator, the noticeable thermal gradient and accompanied mechanical stress inside the gain medium are the most critical issues to be solved. This is due to the fact that the homogeneous doping profile in the active element leads to the exponential decay of the pump light along the longitudinal direction. With an undoped material to effectively serve as a heat sink, the composite crystal has recently proven its feasibility in reducing the spatial gradient of the temperature and the thermally induced mechanical stress [4]–[7]. More recently, the Nd:YAG crystal with increasing doping concentrations was proposed to show that employing the so-called multi-segmented crystal could not only avoid the risk of the thermal fracture inside the laser material, but also maintain the high optical conversion efficiency [8], [9].

Manuscript received March 31, 2014; revised June 10, 2014; accepted June 25, 2014. This work was supported by the National Science Council under Grant NSC-100–2628-M-009-001-MY3.

Y.-J. Huang, W.-Z. Zhuang, and K.-W. Su are with the Department of Electrophysics, National Chiao Tung University, Hsinchu 30010, Taiwan (e-mail: yujenhuang@nctu.edu.tw; edward10517@yahoo.com.tw; sukuanwei@mail.nctu.edu.tw).

Y.-F. Chen is with the Department of Electrophysics, National Chiao Tung University, Hsinchu 30010, Taiwan, and also with the Department of Electronics Engineering, National Chiao Tung University, Hsinchu 30010, Taiwan (e-mail: yfchen@cc.nctu.edu.tw).

Color versions of one or more of the figures in this paper are available online at http://ieeexplore.ieee.org.

Digital Object Identifier 10.1109/JSTQE.2014.2336541

The concept of the master oscillator power amplifier (MOPA) offers another means for boosting the output power of a laser, and it has been widely realized in fiber- and bulk-based architectures [10]–[14]. The required high-power performance can be relatively easily achieved in the MOPA by partially decoupling the problems usually encountered in the high-power laser oscillator, including the possible instability caused by the multi-mode interactions, thermal-lensing effect, and so on. The Nd:YVO_4 crystal, due to the large product of the stimulated emission cross section and the upper-state lifetime, can produce much higher optical gain as compared with other Nd-doped laser materials. To date, most of the Nd:YVO_4 amplifiers are based on the single-pass configuration [12]–[14]. However, some recent works have shown that the double-pass architecture seems to be a more efficient design for scaling the output power of the pulsed oscillator [15], [16]. In this work, an efficient high-power MOPA based on the multi-segmented Nd:YVO_4 crystal is successfully realized for emitting output power greater than one hundred watts in the continuous-wave operation. We first utilize the Fourier eigenfunction expansion method to develop a powerful mathematical technique for analytically solving the heat conduction equation of the anisotropic crystal with a rectangular geometry. Theoretical analysis manifestly reveals that the smoother temperature distribution could be achieved inside the multi-segmented crystal than the conventional composite one. Based on the calculated results, we construct a dual-end-pumped multi-segmented Nd:YVO_4 oscillator for efficiently producing the output power of 50 W. We subsequently design two types of MOPA and make a systematical comparison between both configurations. It is experimentally found that the power gain obtained from the double-pass MOPA is generally larger than that obtained from the single-pass one. Consequently, the output power could be further scaled to reach 108 W at 1064 nm under a total incident pump power of 244 W at 808 nm, corresponding to the optical conversion efficiency of up to 44.3%.

II. Theoretical Analysis on Temperature Distribution

Fig. 1(a) schematically depicts the thermal model of the multi-segmented crystal with a rectangular geometry used for our theoretical analysis, which is end-pumped from two sides. The lengths for each side of the crystal are a, b, and c, respectively. The current multi-segmented crystal is made up of five sections with three doped materials between two undoped end-caps, where the doped parts are characterized by pump absorptions α_1, α_2, and α_3, and heat source densities $q_1(x, y, z)$,

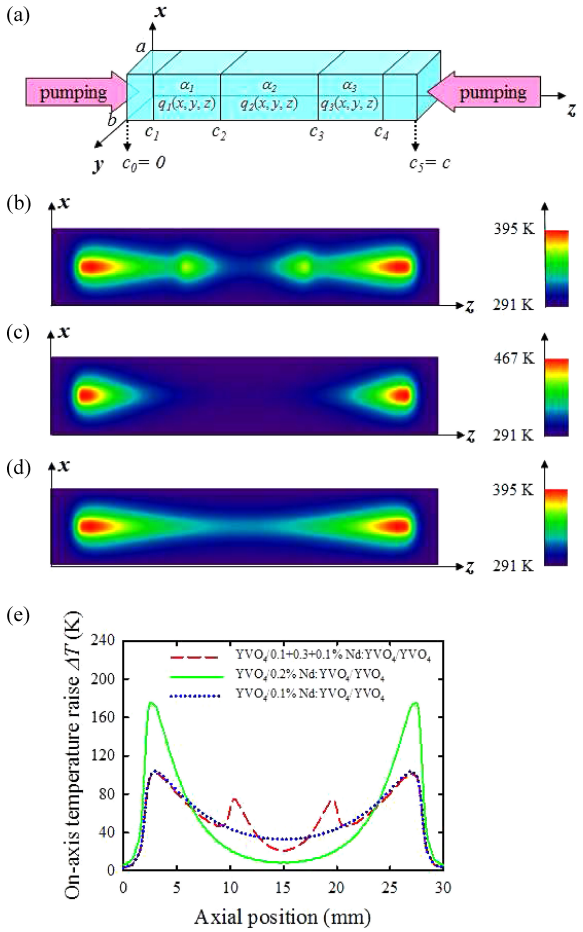

Fig. 1. (a) Configuration of the multi-segmented crystal with a rectangular geometry for the theoretical model; Temperature fields inside the gain medium for: (b) $YVO_4/0.1+0.3+0.1\%$ Nd:YVO_4/YVO_4, (c) YVO_4/0.2% Nd:YVO_4/YVO_4, and (d) YVO_4/0.1% Nd:YVO_4/YVO_4 crystals; (e) On-axis temperature raise as a function of the axial position for the gain medium.

$q_2(x,y,z)$, and $q_3(x,y,z)$, respectively. The z coordinates for every transverse plane are denoted as c_0, c_1, c_2, c_3, c_4, and c_5, respectively. Note that c_0 and c_5 are virtually equal to 0 and c. The temperature field inside a rectangular crystal obeys the heat conduction equation in the Cartesian coordinate, which is given by [17]:

$$K_x\frac{\partial^2 T(x,y,z)}{\partial^2 x}+K_y\frac{\partial^2 T(x,y,z)}{\partial^2 y}+K_z\frac{\partial^2 T(x,y,z)}{\partial^2 z}=-q(x,y,z) \quad (1)$$

where $q(x,y,z)=q_1(x,y,z)+q_2(x,y,z)+q_3(x,y,z)$ is the total heat source density, K_x, K_y and K_z are the thermal conductivity coefficients along the x, y, and z axes, respectively. For the edge-cooled laser crystal, the temperatures at the lateral sides are assumed to be a constant value T_0, while the two end surfaces could be reasonably supposed to be adiabatic since the heat transfer coefficients between the crystal and air are very small. Therefore, the boundary conditions can be expressed as [18]:

$$\begin{aligned} &T(0,y,z)=T_0, T(a,y,z)=T_0\\ &T(x,0,z)=T_0, T(x,b,z)=T_0\\ &\left.\frac{\partial T(x,y,z)}{\partial z}\right|_{z=0}=0, \left.\frac{\partial T(x,y,z)}{\partial z}\right|_{z=c}=0. \end{aligned} \quad (2)$$

The solution to the temperature field subject to the above boundary conditions could be formally represented by a product of three orthogonal sets of eigenfunctions sin[($n\pi/a$)x], sin[($m\pi/b$)y], and cos[($l\pi/c$)z] plus a constant value T_0, that is:

$$T(x,y,z)=\sum_{n=1}^{\infty}\sum_{m=1}^{\infty}\sum_{l=0}^{\infty}A_{nml}\sin\left(\frac{n\pi}{a}x\right)\times\sin\left(\frac{m\pi}{b}y\right)\cos\left(\frac{l\pi}{c}z\right)+T_0 \quad (3)$$

where A_{nml} are the coefficients to be determined. Substituting (3) into (1), the heat conduction equation becomes:

$$\sum_{n=1}^{\infty}\sum_{m=1}^{\infty}\sum_{l=0}^{\infty}B_{nml}\sin\left(\frac{n\pi}{a}x\right)\sin\left(\frac{m\pi}{b}y\right)\cos\left(\frac{l\pi}{c}z\right)=-q(x,y,z) \quad (4)$$

$$B_{nml}=-A_{nml}\left[K_x\left(\frac{n\pi}{a}\right)^2+K_y\left(\frac{m\pi}{b}\right)^2+K_z\left(\frac{l\pi}{c}\right)^2\right]. \quad (5)$$

Using orthogonal properties of sine and cosine functions:

$$\int_0^d\sin\left(\frac{s\pi}{d}x\right)\sin\left(\frac{s'\pi}{d}x\right)dx=\frac{d}{2}\delta_{s,s'} \quad (6)$$

$$\int_0^d\cos\left(\frac{s\pi}{d}x\right)\cos\left(\frac{s'\pi}{d}x\right)dx=\frac{d}{2}\delta_{s,s'} \quad (7)$$

where these are valid for integer numbers of *s* and *s'*, the coefficients A_{nml} can thus be solved as a triple Fourier series for the function *q*(*x*, *y*, *z*):

$$A_{nml}=\frac{8}{abc}\frac{1}{\left[K_x\left(\frac{n\pi}{a}\right)^2+K_y\left(\frac{m\pi}{b}\right)^2+K_z\left(\frac{l\pi}{c}\right)^2\right]}\times\int_0^c\int_0^b\int_0^a q(x,y,z)\sin\left(\frac{n\pi}{a}x\right)\sin\left(\frac{m\pi}{b}y\right)\cos\left(\frac{l\pi}{c}z\right)dxdydz. \quad (8)$$

For a fiber-coupled laser diode, the pump intensity distribution could be approximately expressed as a top-hat function. When the pump beams are injected along the central axis of the

laser crystal, the heat source densities could be expressed as

$$q_i(x,y,z) = [q_{i,L}(x,y,z) + q_{i,R}(x,y,z)] \times H(z-c_i)H(c_{i+1}-z)H \left[\omega_p^2 - \left(x-\frac{a}{2}\right)^2 - \left(y-\frac{b}{2}\right)^2\right] \quad (9)$$

$$q_{i,L}(x,y,z) = \eta \frac{\alpha_i P_{\text{in},L} e^{-\alpha_i (z-c_i)}}{\pi\omega_p^2} \prod_{s=0}^{i-1} e^{-\alpha_s (c_{s+1}-c_s)} \quad (10)$$

$$q_{i,R}(x,y,z) = \eta \frac{\alpha_i P_{\text{in},R} e^{-\alpha_i (c_{i+1}-z)}}{\pi\omega_p^2} \prod_{s'=0}^{N-i} \times e^{-\alpha_{s'} (c_{N+2-s'}-c_{N+1-s'})}, \quad i = 1,2,3 \quad (11)$$

where $H()$ is the Heaviside step function, ω_p is the pump radius, $P_{\text{in},L}$ and $P_{\text{in},R}$ are the incident pump power from the left and right side of the crystal, N is the number of the doped sections, and η is the fractional thermal loading. For a four-level solid-state laser with low doping concentration under the laser condition, the fractional thermal loading can be simply given by the quantum defect $1-\lambda_p/\lambda_L$, where λ_p and λ_L are the pump and lasing wavelengths. Note that we intentionally introduce two null parameters α_0 and α_4 for the general expression of $q_i(x,y,z)$. Substituting (9) into (8) and integrating z from 0 to c, the coefficients A_{nml} can be simplified as

$$A_{nml} = \frac{8}{abc} \frac{(A_{l,L}+A_{l,R})}{\left[K_x\left(\frac{n\pi}{a}\right)^2 + K_y\left(\frac{m\pi}{b}\right)^2 + K_z\left(\frac{l\pi}{c}\right)^2\right]} \times \int_0^b \int_0^a H\left[\omega_p^2 - \left(x-\frac{a}{2}\right)^2 - \left(y-\frac{b}{2}\right)^2\right] \times \sin\left(\frac{n\pi}{a}x\right)\sin\left(\frac{m\pi}{b}y\right) dxdy \quad (12)$$

$$A_{i,L} = \eta \frac{\alpha_i P_{\text{in},L} e^{\alpha_i c_i}}{\pi\omega_p^2(\alpha_i^2 c^2 + l^2\pi^2)} \prod_{s=0}^{i-1} e^{\alpha_s (c_{s+1}-c_s)} \times \left\{ l\pi c \left[e^{-\alpha_i c_{i+1}} \sin\left(\frac{l\pi}{c}c_{i+1}\right) - e^{-\alpha_i c_i}\sin\left(\frac{l\pi}{c}c_i\right)\right] - \alpha_i c^2 \left[e^{-\alpha_i c_{i+1}} \cos\left(\frac{l\pi}{c}c_{i+1}\right) - e^{-\alpha_i c_i}\cos\left(\frac{l\pi}{c}c_i\right)\right]\right\} \quad (13)$$

$$A_{i,R} = \eta \frac{\alpha_i P_{\text{in},R} e^{-\alpha_i c_{i+1}}}{\pi\omega_p^2(\alpha_i^2 c^2 + l^2\pi^2)} \prod_{s'=0}^{N-i} e^{-\alpha_{4-s'} (c_{N+2-s'}-c_{N+1-s'})} \times \left\{ l\pi c \left[e^{\alpha_i c_{i+1}} \sin\left(\frac{l\pi}{c}c_{i+1}\right) - e^{\alpha_i c_i}\sin\left(\frac{l\pi}{c}c_i\right)\right] + \alpha_i c^2 \left[e^{\alpha_i c_{i+1}} \cos\left(\frac{l\pi}{c}c_{i+1}\right) - e^{\alpha_i c_i}\cos\left(\frac{l\pi}{c}c_i\right)\right]\right\} \quad (14)$$

with the following parameters: $N=3$, $a=b=3$ mm, $c_0=0$ mm, $c_1=2$ mm, $c_2=10$ mm, $c_3=20$ mm, $c_4=28$ mm, $c=c_5=30$ mm, $K_x=5.23$ W/(m·K), $K_y=5.1$ W/(m·K), $K_z=5.1$ W/(m·K), $\alpha_1=0.16\ \text{mm}^{-1}$, $\alpha_2=0.48\ \text{mm}^{-1}$, $\alpha_3=0.16\ \text{mm}^{-1}$, $\omega_p=350$ μm, $T_0=291$ K, $\lambda_p=808$ nm, and $\lambda_L=1064$ nm, we calculate the distribution of the temperature field inside the *a*-cut multi-segmented $YVO_4/0.1+0.3+0.1\%$ Nd:YVO_4/YVO_4 crystal for the case of $P_{\text{in},L}=P_{\text{in},R}=54$ W, as shown in Fig. 1(b). For the purpose of comparison, the temperature distributions for the conventional composite YVO_4/0.2% Nd:YVO_4/YVO_4 and YVO_4/0.1% Nd:YVO_4/YVO_4 crystals with the same dimensions are also calculated, as displayed in Fig. 1(c) and (d). The values of *n* and *m* used for the calculation are both from 1 to 41 for symmetry, while for *l* it is ranged from 0 to 80. Our calculation has shown that these chosen index values are sufficient for the temperature variation within 10^{-2} while keeping the computation time to be not more than ten minutes. We also compare the Fourier eigenfunction expansion method with the finite-element analysis [17] and find that only a small difference between these two approaches is observed. However, the computation time for the Fourier eigenfunction expansion method is several times faster than that for the finite-element analysis. Fig. 1(e) illustrates the on-axis temperature raise with respect to the axial position for these three types of crystal. It can be clearly concluded that not only the maximum temperature raise could be effectually reduced, but also the heat could be spread more uniformly inside the multi-segmented crystal. The theoretical analysis is consistent with the experimental results on the focal length of the thermal lens investigated in our previous study [19]. This indicates that the multi-segmented crystal is a promising approach for developing a high-power end-pumped laser, as will be further experimentally demonstrated as follows. It is worthwhile to mention that the similar analysis has been previously performed for the multi-segmented Nd:YAG rod with a cylindrical geometry, where the temperature field is expanded by a series of Bessel functions [20], and the potential for such crystal design in power scaling was experimentally realized. We also want to address that if the pump intensity distribution does not follow the top-hat function, the heat source densities (9)–(11) and thus the coefficients A_{nml} expressed in (12)–(14) should be modified, which would result in slightly different temperature values. For example, we have computationally found that the temperature peak value for the Gaussian pump intensity distribution is 4–6% higher than the value obtained from the top-hat pumping, whereas the morphologies of temperature distribution are quite similar to each other.

III. Performance of the Dual-End-Pumped Multi-Segmented Oscillator

The experimental arrangement of high-power dual-end-pumped continuous-wave oscillator with the five-segmented Nd:YVO_4 crystal is schematically shown in Fig. 2(a). A plane mirror with anti-reflection at 808 nm on the entrance side and high reflection at 1064 nm as well as high transmission at 808 nm on the other side was employed as the front mirror. The coating characteristic of the folding mirror was the same as that of the front mirror, except that the angle of incidence was designed to be 45°. The *a*-cut $YVO_4/0.1+0.3+0.1\%$ Nd:YVO_4/YVO_4

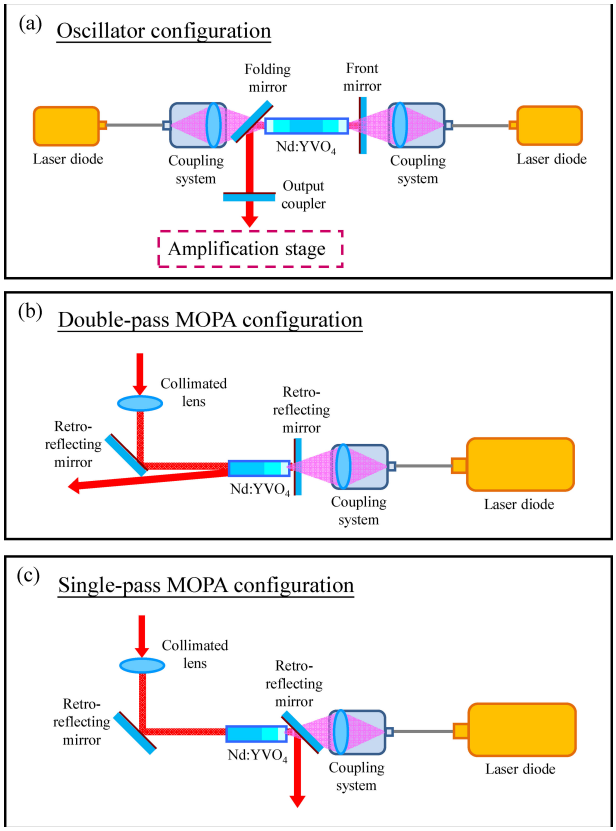

Fig. 2. Experimental setup for the: (a) diode-pumped $YVO_4/0.1 + 0.3 + 0.1\%$ Nd:YVO_4/YVO_4 laser with dual-end pumping, (b) double-pass MOPA configuration, and (c) single-pass MOPA configuration.

crystal consisted of two undoped end-caps with the lengths of 2 mm, and three active parts with the lengths of 8, 10, and 8 mm, corresponding to the doping concentrations of 0.1, 0.3, and 0.1%, respectively. Our multi-segmented crystal was designed for the dual-end pumping to make the generated heat more uniform inside the gain medium, and thus a superior laser performance could be achieved. The transverse cross section of the crystal is 3 mm $\times$ 3 mm. Both end faces of the gain medium were coated to be anti-reflective at pump and lasing wavelengths. The laser crystal was wrapped with indium foil and mounted in a water-cooled copper holder with the temperature at 18°C. A flat mirror with the reflectivity of 85% at 1064 nm was utilized as the output coupler. The pump sources were two 808-nm fiber-coupled laser diodes with the nominal powers of 60 W for each. The numerical aperture and core diameter of the coupling fiber were 0.22 and 600 μm, respectively. The pump beams were reimaged into the laser crystal with the spot radii of 350 μm through two convex lenses with the focal lengths of 25.4 mm and the coupling efficiencies of 95%. The cavity length of the whole resonator was around 70 mm.

First of all, the laser oscillator was carefully optimized for the maximum output power under an incident pump power of 108 W. Then, the output power at 1064 nm as a function of the incident pump power at 808 nm was measured, as exhibited in Fig. 3. The pump threshold is around 5.2 W, and the maximum

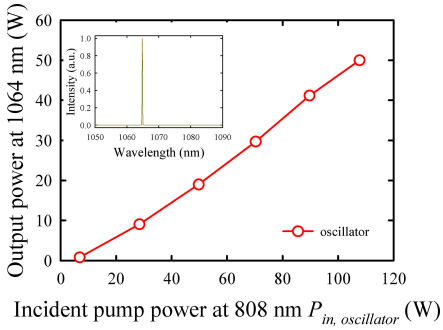

Fig. 3. Dependence of the output power at 1064 nm on the incident pump power at 808 nm for the diode-pumped $YVO_4/0.1 + 0.3 + 0.1\%$ Nd:YVO_4/YVO_4 laser. Inset: corresponding optical spectrum for the laser output.

output power as high as 50 W is efficiently generated under an incident pump power of 108 W. The corresponding slope and optical conversion efficiencies are evaluated to be 48.6 and 46.3%, respectively. The beam quality factor was measured to be better than 1.8 with a knife-edge method. The output radiation was linearly polarized along the c axis of the Nd:YVO_4 crystal, and the extinction ratio was found to be larger than 200:1. More importantly, no thermal fracture inside the gain medium was observed during the experiment. Combined with our previous studies [19], it can be clearly deduced that utilizing the multi-segmented crystal is practically valuable in scaling the output power for diode-end-pumped laser system without introducing considerable thermally accompanied detrimental effects. The spectral information for the developed Nd:YVO_4 laser was recorded with an optical spectrum analyzer (Advantest 8381A) with the resolution of 0.1 nm. The central wavelength of the laser output locates at 1064.8 nm with the full width at half maximum of approximately 0.3 nm, as displayed in the inset of Fig. 3. In the following section, we design two types of MOPA to further scale the output power at 1064 nm.

IV. Comparative Investigation Between Double- and Single-Pass MOPA Configurations

Fig. 2(b) and (c) schematically depict the experimental layouts for the MOPAs with double- and single-pass configurations, respectively. All retro-reflecting mirrors were coated for high reflection at 1064 nm. The same coupling system was also utilized in the amplification stage, except that the magnified ratio is different. The amplified medium was a three-segmented Nd:YVO_4 crystal with a 2-mm-long undoped YVO_4 crystal bonded to a 0.1-% doping Nd:YVO_4 crystal with the length of 8 mm, and followed by a 0.3-% doping material with the length of 5 mm. The active medium was wrapped with indium foil and mounted in a water-cooled copper block at the temperature at 18°C. An 145-W fiber-coupled laser diode at 808 nm was employed to pump the Nd:YVO_4 crystal with the spot radius of 800 μm. The laser beam emitted from the master oscillator was collimated by a plano-convex lens with the focal length of 80 mm. For the double-pass MOPA configuration shown in Fig. 2(b), the laser beam propagated the amplified medium twice achieved

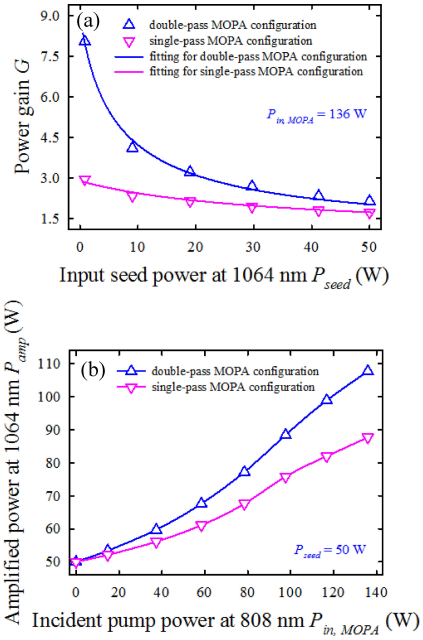

Fig. 4. (a) Power gains as a function of the input seed power and (b) output powers versus the incident pump power at the amplification stage for both configurations.

by a retro-reflecting mirror with a small inclined angle; while only one trip through the Nd:YVO_4 crystal for the laser beam was adopted in the single-pass MOPA architecture described in Fig. 2(c). It should be point out that the crystal structure used in the amplifier stage was different from that utilized in the oscillator stage. This is because the input seed and amplified radiations pass the same side of the active medium in our double-pass MOPA configuration aimed for single end pumping from the opposite face of the crystal. Moreover, if the Nd:YVO_4 crystal with a dimension of 3 mm × 3 mm × 30 mm (as used in the oscillator stage) was adopted, the amplified laser radiation would be easily blocked by the surrounded copper holder, resulting in a significant decrease of the output power.

Initially, we varied the input seed power from the master oscillator to systematically compare the amplified abilities for two configurations with the incident pump power at the amplification stage to be fixed at 136 W. Fig. 4(a) illustrates the power gains for the double- and single-pass MOPA configurations versus the incident pump power at the amplification stage. The power gain G is defined as the ratio of the amplified power $P_{\rm amp}$ to the input seed power $P_{\rm seed}$ at 1064 nm. It can be obviously seen that the power gain achieved in the double-pass MOPA architecture is generally larger than that obtained from the single-pass MOPA architecture, especially for the low input seed power. Experimental results also manifestly reveal that the power gain decreases by increasing the input seed power for both configurations, this is a typical behavior for the power amplifier [13], [15], [16]. When the input seed power is changed from 0.8 to 50 W, the power gains are experimentally found to decrease from 8 to 2.16 for the double-pass MOPA frame and from 2.95 to 1.76 for the single-pass MOPA frame, respectively.

In order to well characterize these two types of power amplifier, the gain curves are fitted by a Frantz-Nodvik model for a continuous-wave operation [21], [22]:

$$G = \frac{P_{\rm amp}}{P_{\rm seed}} = \frac{P_{\rm sat}}{P_{\rm seed}} \ln\left\{1 + G_0\left[\exp\left(\frac{P_{\rm seed}}{P_{\rm sat}}\right) - 1\right]\right\} \quad (15)$$

where $P_{\rm sat}$ is the saturation parameter and G_0 is the small-signal gain. For the single-pass MOPA configuration, the saturation parameter and small-signal gain are characterized by $P_{\rm sat} = 45$ W and $G_0 = 2.9$, respectively. On the other hand, $P_{\rm sat} = 25$ W and $G_0 = 9$ are obtained with the double-pass MOPA configuration, confirming the relatively high-gain and low saturation power provided by this amplifier structure.

We further investigated the dependence of the amplified power on the incident pump power at the amplification stage when the input seed power was fixed to be 50 W, as exhibited in Fig. 4(b). Under an incident pump power of 136 W, the amplified power for the single-pass MOPA configuration is acquired to be 88 W. On the other hand, the amplified power as high as 108 W is achieved for the double-pass MOPA frame under an incident pump power of 136 W, which is remarkably larger than that obtained from single-pass MOPA frame. The beam quality factors were generally better than 2.2 and the polarization remained linear after either single- or double-pass MOPA configurations. According to the results demonstrated here, it is believed that employing the multi-segmented crystal combined with the double-pass MOPA configuration is suitable for accomplishing a reliable, efficient high-power diode-end-pumped laser system.

V. Conclusion

In summary, a novel Nd:YVO_4 crystal with multiple doping concentrations has been originally fabricated for constructing a high-power MOPA system. The temperature field inside a rectangular-shaped laser crystal has been precisely calculated by a powerful mathematical model on the basis of the Fourier eigenfunction expansion method. Based on the theoretical analysis, a reliable continuous-wave $YVO_4/0.1 + 0.3 + 0.1\%$ Nd:YVO_4/YVO_4 oscillator is successfully developed to generate the output power of up to 50 W with dual-end pumping. Moreover, we have designed a double-pass MOPA to remarkably boost the laser power to reach 108 W under a total incident pump power of 244 W, corresponding to the optical conversion efficiency of 44.3%.

References

[1] N. Hodgson, K. Griswold, W. Jordan, S. L. Knapp, A. A. Peirce, C. C. Pohalski, E. Cheng, J. Cole, D. R. Dudley, A. B. Petersen, and W. L. Nighanjr, "High power TEM_{00} mode operation of diode-pumped solid state lasers," *Proc. SPIE*, vol. 3611, pp. 119–131, Jan. 1999.

[2] N. Hodgson, M. Li, A. Held, and A. Krueger, "Diode-pumped TEM_{00} mode solid state lasers and their micromachining applications," *Proc. SPIE*, vol. 4977, pp. 281–294, Jan. 2003.

[3] S. R. Bowman, "High-power diode-pumped solid-state lasers," *Opt. Eng.*, vol. 52, art. no. 021012, Feb. 2013.

[4] F. Hanson, "Improved laser performance at 946 and 473 nm from a composite Nd:$Y_3Al_5O_{12}$ rod," *Appl. Phys. Lett.*, vol. 66, pp. 3549–3551, Jun. 1995.

[5] M. Tsunekane, N. Taguchi, T. Kasamatsu, and H. Inaba, "Analytical and experimental studies on the characteristics of composite solid-state laser rods in diode-end-pumped geometry," *IEEE J. Sel. Topics Quantum Electron.*, vol. 3, no. 1, pp. 9–18, Feb. 1997.

[6] X. Li, X. Yu, F. Chen, R. Yan, M. Luo, J. Yu, and D. Chen, "Power scaling of directly dual-end-pumped Nd:$GdVO_4$ laser using grown-together composite crystal," *Opt. Exp.*, vol. 18, pp. 7407–7414, Mar. 2010.

[7] Y. J. Huang, Y. P. Huang, H. C. Liang, K. W. Su, Y. F. Chen, and K. F. Huang, "Comparative study between conventional and diffusion-bonded Nd-doped vanadate crystals in the passively mode-locked operation," *Opt. Exp.*, vol. 18, pp. 9518–9524, Apr. 2010.

[8] R. Wilhelm, D. Freiburg, M. Frede, and D. Kracht, "End-pumped Nd:YAG laser with a longitudinal hyperbolic dopant concentration profile," *Opt. Exp.*, vol. 16, pp. 20106–20116, Nov. 2008.

[9] R. Wilhelm, M. Frede, and D. Kracht, "Power scaling of end-pumped solid-state rod lasers by longitudinal dopant concentration gradients," *IEEE J. Quantum Electron.*, vol. 44, no. 3, pp. 232–244, Mar. 2008.

[10] Y. Jeong, J. Nilsson, J. K. Sahu, D. B. S. Soh, C. Alegria, P. Dupriez, C. A. Codemard, D. N. Payne, R. Horley, L. M. B. Hickey, L. Wanzcyk, C. E. Chryssou, J. A. Alvarez-Chavez, and P. W. Turner, "Single-frequency, single-mode, plane-polarized ytterbium-doped fiber master oscillator power amplifier source with 264 W of output power," *Opt. Lett.*, vol. 30, pp. 459–461, Mar. 2005.

[11] M. Hildebrandt, M. Frede, P. Kwee, B. Willke, and D. Kracht, "Single-frequency master-oscillator photonic crystal fiber amplifier with 148 W output power," *Opt. Exp.*, vol. 14, pp. 11071–11076, Nov. 2006.

[12] J. W. Kim, M. J. Yarrow, and W. A. Clarkson, "High power single-frequency continuous-wave Nd:YVO_4 master-oscillator power amplifier," *Appl. Phys. B*, vol. 85, pp. 539–543, Dec. 2006.

[13] X. Yan, Q. Liu, X. Fu, Y. Wang, L. Huang, D. Wang, and M. Gong, "A 108 W, 500 kHz Q-switching Nd:YVO_4 laser with the MOPA configuration," *Opt. Exp.*, vol. 16, pp. 3356–3361, Mar. 2008.

[14] S. Yan, X. Yan, H. Yu, L. Zhang, L. Guo, W. Sun, W. Hou, and X. Lin, "A high power picosecond Nd:YVO_4 master oscillator power amplifier system pumper by 880 nm diodes," *Laser Phys.*, vol. 23, art. no. 075302, Jul. 2013.

[15] A. Agnesi, L. Carrà, R. Piccoli, F. Pirzio, and G. Reali, "Nd:YVO_4 amplifier for ultrafast low-power lasers," *Opt. Lett.*, vol. 37, pp. 3612–3614, Sep. 2012.

[16] X. Délen, F. Balembois, and P. Georges, "Direct amplification of a nanosecond laser diode in a high gain diode-pumped Nd:YVO_4 amplifier," *Opt. Lett.*, vol. 39, pp. 997–1000, Feb. 2014.

[17] Z. Xiong, Z. G. Li, N. Moore, W. L. Huang, and G. C. Lim, "Detailed investigation of thermal effects in longitudinally diode-pumped Nd:YVO_4 lasers," *IEEE J. Quantum Electron.*, vol. 39, no. 8, pp. 979–986, Aug. 2003.

[18] P. Shi, W. Chen, L. Li, and A. Gan, "Semianalytical thermal analysis on a Nd:YVO_4 crystal," *Appl. Opt.*, vol. 46, pp. 4046–4051, Jul. 2007.

[19] Y. J. Huang and Y. F. Chen, "High-power diode-end-pumped laser with multi-segmented Nd-doped yttrium vanadate," *Opt. Exp.*, vol. 21, pp. 16063–16068, Jul. 2013.

[20] R. Wilhelm, D. Freiburg, M. Frede, D. Kracht, and C. Fallnich, "Design and comparison of composite rod crystals for power scaling of diode end-pumped Nd:YAG lasers," *Opt. Exp.*, vol. 17, pp. 8229–8236, May 2009.

[21] L. M. Frantz and J. S. Nodvik, "Theory of pulse propagation in a laser amplifier," *J. Appl. Phys.*, vol. 34, pp. 2346–2349, Aug. 1963.

[22] W. Koechner, *Solid-State Laser Engineering*, 6th ed. Berlin, Germary: Springer-Verlag, 2005, ch. 4.

Yu-Jen Huang was born in Hualien, Taiwan, in 1987. He received the B.S. and the Ph.D. degrees in electrophysics from National Chiao Tung University, Hsinchu, Taiwan, in 2009 and 2013, respectively. He is currently a Postdoctoral Research Fellow in the Department of Electrophysics, National Chiao Tung University. His research interests include the physics and technology of diode-pumped solid-state lasers and nonlinear frequency conversion. Dr. Huang is a Member of the Optical Society of America.

Wei-Zhe Zhuang was born in Taichung, Taiwan, in 1986. He received the B.S. and Ph.D. degrees in electrophysics from National Chiao Tung University, Hsinchu, Taiwan, in 2008 and 2013, respectively.

He is currently a Postdoctoral Research Fellow with the Department of Electrophysics, National Chiao Tung University. His research interests include fiber lasers and diode-pumped solid-state lasers.

Kuan-Wei Su was born in Kaohsiung, Taiwan, in 1979. He received the B.S. degree in physics from National Cheng Kung University, Tainan, Taiwan, in 2001, and the M.S. and Ph.D. degrees in electrophysics from National Chiao Tung University, Hsinchu, Taiwan, in 2004 and 2007, respectively.

He is currently an Associate Professor in the Department of Electrophysics, National Chiao Tung University. His research interests include fiber lasers, diode-pumped solid-state lasers, and high-speed dynamics of lasers and matter.

Dr. Su is a Member of the Optical Society of America.

Yung-Fu Chen was born in Lukang, Taiwan, in 1968. He received the B.S. and Ph.D. degrees in electronics engineering from National Chiao Tung University, Hsinchu, Taiwan, in 1990 and 1994, respectively.

Since 1994, he was with Precision Instrument Development Center, National Science Council, Taiwan, where his research mainly concerns the development of diode-pumped solid-state laser as well as quantitative analysis in surface electron spectroscopy. Since 1999, he was with National Chiao Tung University (NCTU) as the Associate Professor in the Department of Electrophysics. Since 2001, he was promoted to be the Professor in NCTU. He had served as the Executive Dean in the College of Science, NCTU, between 2006 and 2007. He had also served as the Chair in the Department of Electrophysics between 2011 and 2013. Since 2011, he has been identified as the Distinguished Professor. He has received several outstanding awards, such as Sun-Yet-Sen academic award for excellent papers in 2008, Outstanding Research Award from the National Science Council in 2004 and 2011, and Outstanding Honorary Award from the Ho C.T. Education Foundation in 2011. His main research interests include laser physics, solid-state lasers, Q-switched lasers, mode-locked lasers, and transverse pattern formation in microchip lasers.

Dr. Chen is a Member of the Optical Society of America and the IEEE Photonics Society. Currently, he serves as the Associate Editor for the *Optics Express*.